IJMMM International Journal of Minerals, Metallurgy and Materials 矿物冶金与材料学报（英文版）

Fatigue limit assessment of a 6061 aluminum alloy based on infrared thermography and steady ratcheting effect

Ru-yi Feng, Wen-xian Wang, Zhi-feng Yan, Deng-hui Wang, Shi-peng Wan, and Ning Shi

Cite this article as:
Ru-yi Feng, Wen-xian Wang, Zhi-feng Yan, Deng-hui Wang, Shi-peng Wan, and Ning Shi, Fatigue limit assessment of a 6061 aluminum alloy based on infrared thermography and steady ratcheting effect, *Int. J. Miner. Metall. Mater.*, 27(2020), No. 9, pp. 1301-1308. https://doi.org/10.1007/s12613-019-1942-2

View the article online at SpringerLink or IJMMM Webpage.

International Journal of Minerals, Metallurgy and Materials
Volume 27, Number 9, September 2020, Page 1301
https://doi.org/10.1007/s12613-019-1942-2

Fatigue limit assessment of a 6061 aluminum alloy based on infrared thermography and steady ratcheting effect

Ru-yi Feng[1)], *Wen-xian Wang*[1,2,3)], *Zhi-feng Yan*[1,2,3)], *Deng-hui Wang*[1)], *Shi-peng Wan*[1)], *and Ning Shi*[1)]

1) College of Materials Science and Engineering, Taiyuan University of Technology, Taiyuan 030024, China
2) Key Laboratory of Interface Science and Engineering in Advanced Materials, Ministry of Education, Taiyuan University of Technology, Taiyuan 030024, China
3) Shanxi Key Laboratory of Advanced Magnesium-based Materials, Taiyuan University of Technology, Taiyuan 030024, China
(Received: 4 October 2019; revised: 3 November 2019; accepted: 1 December 2019)

Abstract: To quickly predict the fatigue limit of 6061 aluminum alloy, two assessment methods based on the temperature evolution and the steady ratcheting strain difference under cyclic loading, respectively, were proposed. The temperature evolutions during static and cyclic loadings were both measured by infrared thermography. Fatigue tests show that the temperature evolution was closely related to the cyclic loading, and the cyclic loading range can be divided into three sections according to the regular of temperature evolution in different section. The mechanism of temperature evolution under different cyclic loadings was also analyzed due to the thermoelastic, viscous, and thermoplastic effects. Additionally, ratcheting strain under cyclic loading was also measured, and the results show that the evolution of the ratcheting strain under cyclic loading above the fatigue limit undergone three stages: the first increasing stage, the second steady state, and the final abrupt increase stage. The fatigue limit of the 6061 aluminum alloy was quickly estimated based on transition point of linear fitting of temperature increase and the steady value of ratcheting strain difference. Besides, it is feasible and quick of the two methods by the proof of the traditional *S–N* curve.

Keywords: 6061 Aluminum; temperature evolution; fatigue limit; ratcheting strain

1. Introduction

The wide use of aluminum alloys as various structures and mechanical components in the military and aerospace fields is promising due to their low density, high specific strength, and good plasticity [1–2]. In these applications, most of the components are inevitably serviced under cyclic loading and are more inclined to suddenly rupture, which causes great loss or disaster [3]. Fatigue failure under cyclic loading is a process of damage accumulation in which most of the plastic work is consumed in the form of heat, causing an increase in the surface temperature [4]. Therefore, it is of great significance to study the relationship between the change in surface temperature and fatigue cyclic loading. Infrared thermography (IRT), detecting heat waves generated by materials during dynamic loading with the infrared camera, has been efficiently used to record the surface temperature evolution and investigate the thermomechanical behavior of materials in a wide range of fields due to its real-time and non-contact advantages [5]. Fan *et al.* [6] determined the fatigue behavior and established an energetic model to predict the residual life of Q235 steel by IRT. Cui *et al.* [7] used IRT to measure the fatigue crack growth of electron beam welded joints of the AZ31B magnesium alloy under cyclic loading and proposed a theoretical model to present the distribution of dissipated energy from the crack tip. Xu *et al.* [8] investigated the temperature evolution and predicted the fatigue life of the AZ31B magnesium alloys loaded under three-point-bending. Yan *et al.* [9] studied the effect of anisotropy on the fatigue and tensile behavior of a 5A06 aluminum alloy based on IRT and found a longitudinal specimen has higher fatigue strength life than the transverse specimen. Bandeira *et al.* [10] assessed the fatigue behavior of bonded joints using a thermographic acquisition system and confirmed that it is an alternative approach to evaluate the fatigue strength. Yang *et al.* [11] proposed an approach to rapidly predict the high-cycle fatigue reliability (three-parameter *P–S–N* curves) of metallic materials and developed a calculation model of energy dissipation based on quantitative thermography methodology. However, little attention has been given to the temperature evolution of a 6061 aluminum alloy, especially at wider cyclic loading level. Thus, analyzing the temperature evolu-

Corresponding author: Wen-xian Wang E-mail: wangwenxian@tyut.edu.cn

tion and fatigue limit of a 6061 aluminum alloy under cyclic loading based on the IRT method is imperative.

During service, asymmetric cyclic loading may cause strain accumulation and additional plastic damage, which is known as ratcheting [12–13]. Essential deformation occurred on the engineering materials may lead to the catastrophic failure because of the ratcheting strain and damage accumulation. In recent years, some researchers have investigated the ratcheting phenomenon of aluminum and magnesium alloys [13–17]. They mostly investigated the effect of various parameters such as mean stress, stress amplitude, and pre-ratcheting strain to fatigue or tensile property at low cycle fatigue test. Very little literature has reported the ratcheting strain behavior of the 6061 aluminum alloy under different cyclic loading levels or investigated the fatigue limit based on the ratcheting strain evolution.

In this paper, the temperature and ratcheting strain evolutions of the 6061 aluminum alloy under fatigue test with cyclic loading were investigated, and the fatigue limit was evaluated based on IRT and the steady ratcheting strain.

2. Experimental

The material was a rolled, 4-mm-thick plate. The chemical composition and the tensile property of 6061 aluminum alloy are shown in Tables 1 and 2, respectively. Fig. 1 shows the initial microstructures of the 6061 aluminum alloy. The alloy has an uneven grain size, and there are precipitates in and between grains.

Table 1. Chemical composition of the 6061 aluminum alloy

wt%

Mg	Si	Mn	Cu	Zn	Ti	Cr	Fe	Al
1.054	0.621	0.081	0.236	0.007	0.021	0.138	0.35	Bal.

Table 2. Tensile properties of the 6061 aluminum alloy

Tensile strength / MPa	Yield strength / MPa	Elongation / %
230	180	21

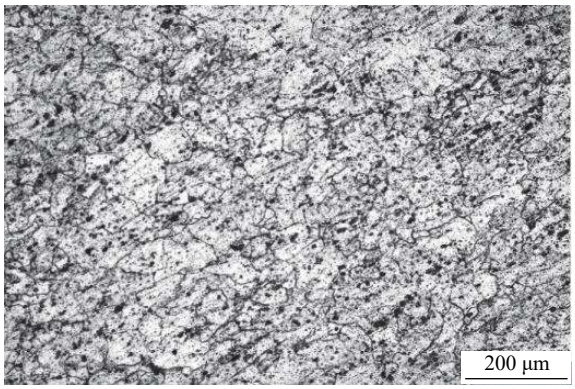

Fig. 1. Initial microstructure of the 6061 aluminum alloy.

The specimens were machined via wire electrode cutting, and the size of specimens for the tensile and fatigue tests is shown in Fig. 2. The specimens were polished like a mirror surface with metallographic sandpaper to remove contaminants and delay the crack initiation. Before the cyclic loading test, a black thin opaque paint layer was covered on the surface to increase the thermal emissivity and reduce background reflection, aiming to improve the accuracy of the temperature measurement.

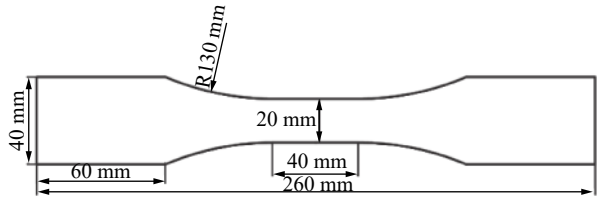

Fig. 2. Size of the samples for the fatigue and tensile test.

The tensile test was performed on a DNS-100 universal testing machine at a stress rate of 5 mm·min^{-1}. The fatigue test was performed using a fully PLG-200D high frequency electromagnetic resonance fatigue test system with a sinusoidal-waveform-stress-controlled mode at stress ratio of 0.1 and frequency of about 100 Hz. The maximum cyclic loading ranged from 10 to 230 MPa. The specimens were under cyclic loading until failure or the number of cycles up to 10^7 without fracture. At the same time, the cyclic strain and ratcheting strain curves were conducted by an axial extensometer with a 25 mm gauge length.

An InfraTec VarioCAM hr infrared camera, with 1024 × 768 pixels and temperature sensitivity greater than 0.08 K at 303 K, was used to record the temperature evolution of samples. The temperature data was analyzed with IRBIS3 software. The temperature increment (ΔT) was calculated by $\Delta T = T - T_0$ (where T and T_0 are the instantaneous temperature and initial temperature on the surface of the sample, respectively)

3. Results and discussion

3.1. Heat generation during plastic deformation

The dissipation, internal energy variation, and possible thermomechanical effect are involved in the cyclic loading, and the thermomechanical equation is [18]:

$$Q = \Delta W = \int_{\sigma_{min}}^{\sigma_{max}} f(\varepsilon)\mathrm{d}\sigma \quad (1)$$

where W is the mechanical energy of the material under cyclic loading when a unit volume is expended, ΔW is the part of W that transforms into the heat Q, $f(\varepsilon)$ is the strain (ε) function, and σ_{max} and σ_{min} are the maximum and minimum cyclic loadings in the fatigue test, respectively. Therefore, the area of the hysteresis loop is closely related to the heat generation.

Materials naturally conduct heat and the energy balance in

two dimensions is [19]:

$$\rho C_P \frac{\partial T}{\partial t} = \kappa\left(\frac{\partial^2 T}{\partial x^2} + \frac{\partial^2 T}{\partial y^2}\right) + Q' \tag{2}$$

where ρ is the density of material, C_P is the heat capacity at constant pressure, T is the specimen temperature, t is the time, κ is thermal conductivity, x and y are the distance between the two adjacent pixels in two directions, and Q' is the heat-dissipation rate.

3.2. Temperature evolution during static tensile test

Kelvin explained the phenomenon of material cooling with an elastic volume increase as the thermoelastic effect. Lee and Shaue [20] used Kelvin's theory to investigate the temperature evolution of the 2024-T3 and 7075-T6 alloys induced by a thermomechanical effect under uniaxial tensile loading. The temperature evolution and tensile curve during tensile test of the 6061 aluminum alloy are shown in Fig. 3. The solid red and dotted black lines are the temperature evolution curves and the stress–strain curve, respectively. There are four stages in the temperature evolution curve: I—a first decrease, II—a reversible increase, III—an abrupt increase, and IV—a drop stage. Fig 4 shows the instantaneous infrared thermograms corresponding to the above four stages.

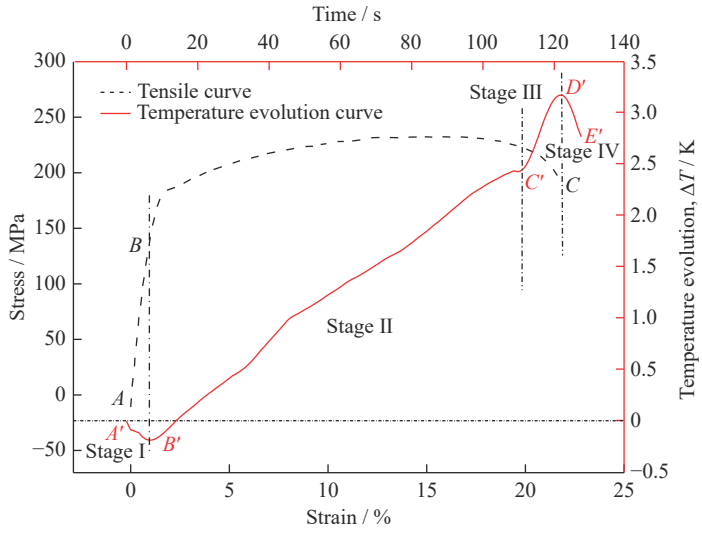

Fig. 3. Temperature evolution and stress–strain curve during the static tensile test.

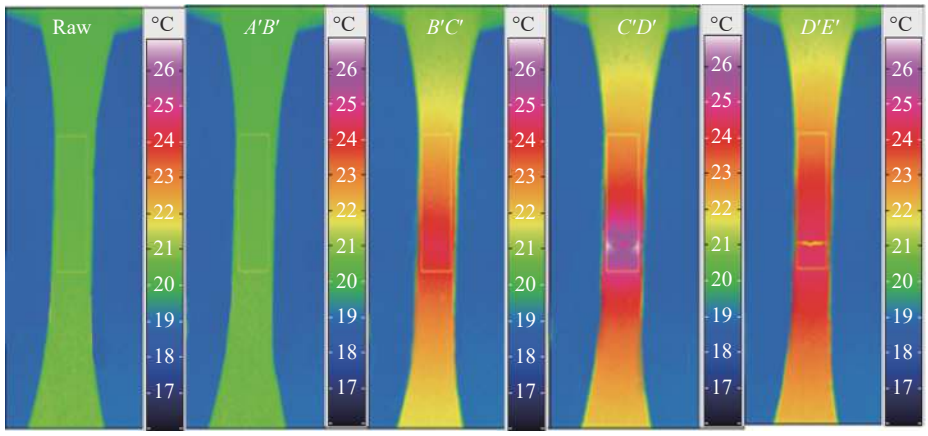

Fig. 4. Instantaneous infrared thermograms corresponding to the different temperature evolution stages shown in Fig. 3.

In Fig. 3, L_{AB} (the AB line) is the elastic deformation process, corresponding to the temperature decrease due to the thermoelastic effect just as $L_{A'B'}$ shows. The plastic work converts to heat causing the temperature increase as $L_{B'C'}$ shows when plastic deformation occurs. In stage III, the temperature increases suddenly due to the macrocrack initiation, causing a large amount of heat at the crack tip. The temperature gradually decreases at stage IV because of the heat conduction.

When the sample is under static stress, there is only one principal stress along the same axial direction of sample. The temperature evolution can be represented by the following

equation [21]:

$$\Delta T = -\frac{\alpha T_0}{\rho C_P}\sigma \tag{3}$$

where α is the coefficient of linear thermal expansion, and σ is the stress.

In the static tensile test, α is 23.6 × 10^{-6} K^{-1}, ρ is 2.75 g·cm^{-3} and C_P is 900 J·kg^{-1}·K^{-1}. The ambient temperature was 298 K and σ in point B of Fig. 3 is 125 MPa. As a result, the calculated value of ΔT is −0.35 K, and the experimental value is −0.24 K; the relative error based on theory value is 31 %, indicating good compliance.

3.3. Temperature evolution during the fatigue test

The temperature evolution of the 6061 Al alloy in the cyclic loading test is different from the static tensile test. When the maximum cyclic loading was less than 70 MPa, the samples did not break, and the temperature decreased first in these cyclic loadings due to the thermoelastic effect (Fig. 5(a)), which is the same tendency in the first stage of the static tensile test. However, the samples fracture when the maximum cyclic loading is between 80 and 180 MPa. Only about the first 2 h of temperature evolution are recorded as shown in Fig. 5(b), during which three stages occurred: I—initial increase, II—steep decrease, and III—steady state. The temperature increases in this cyclic loading level can be attributed to a viscous effect. According to the Voig–Kelvin model, the constitutive equation is expressed as follows [22]:

$$\sigma_{max} = E\varepsilon + F\dot{\varepsilon} \tag{4}$$

where E and F mean the coefficients of elastic and viscous, ε and $\dot{\varepsilon}$ are the strain and rate of strain, $E\varepsilon$ is the elastic strain, and $F\dot{\varepsilon}$ is the viscous strain. The temperature evolution attributed to the thermoelastic effect is neglected when plastic deformation occurs, so a small increase in the temperature due to the thermoplastic effect is expressed as:

$$\Delta T = aF\dot{\varepsilon} + b \tag{5}$$

where a and b represent the slope and intercept of the line, respectively.

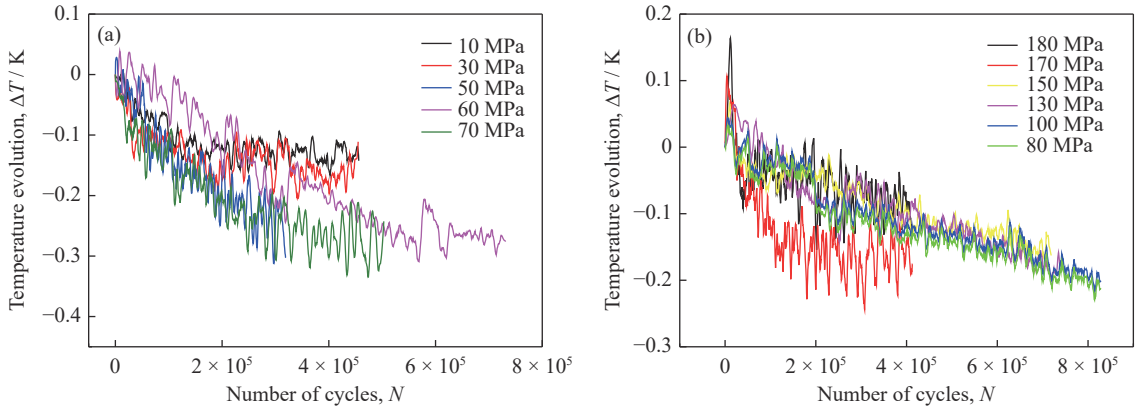

Fig. 5. Temperature evolution curve of the sample under different maximum cyclic loadings: (a) below 70 MPa; (b) between 80 and 180 MPa.

Fig. 6(a) shows the temperature evolution of samples under maximum cyclic loading ranging from 180 to 230 MPa. The temperature evolution curve consists of five stages: I—initial increase, II—steep decrease, III—steady state, IV—an abrupt increase, and V—final drop. The temperature increases in the first stage along with the increasing in cyclic loading. The maximum cyclic loading of 220 MPa clearly exhibits the five stages as shown in Fig. 6(b). Stage I shows the rapid increase in temperature at about 2 × 10^4 cycles. Based on the inelastic effect, local plastic deformation occurs, causing the rate of heat generation to be greater than that of heat conduction, resulting in the temperature increase. When the difference of the two rates reaches a maximum, the temperature in stage I also reaches a maximum. After limited plastic deformation and work hardening, the temperature decreases steeply because of the heat conduction effect, as shown in stage II. In stage III, the temperature maintains stability because of the balance in the rates of heat conduction and heat generation. The temperature increases abruptly when a macrocrack forms and the plastic energy converts to heat as shown at stage IV, and the temperature decreases due to the conduction of heat to the environment as shown at stage V. The corresponding instantaneous infrared thermograms of above five stages are shown in Fig. 7. The temperature significantly increases in stage I when the maximum cyclic loading is above 180 MPa and the increase in temperature in the first stage is due to the thermoplastic effect [23]:

$$\Delta T_i = \frac{\eta}{\rho C_p}\int_{\varepsilon_1}^{\varepsilon_2} f(\sigma)\mathrm{d}\varepsilon \tag{6}$$

where ΔT_i is the temperature variation caused by the thermoplastic effect in each cycle, i is the number of cycles, η is the work-heat transfer coefficient, $f(\sigma)$ is the cyclic loading equation, and ε_1 and ε_2 are the minimum and maximum value of strain in hysteresis loop, respectively.

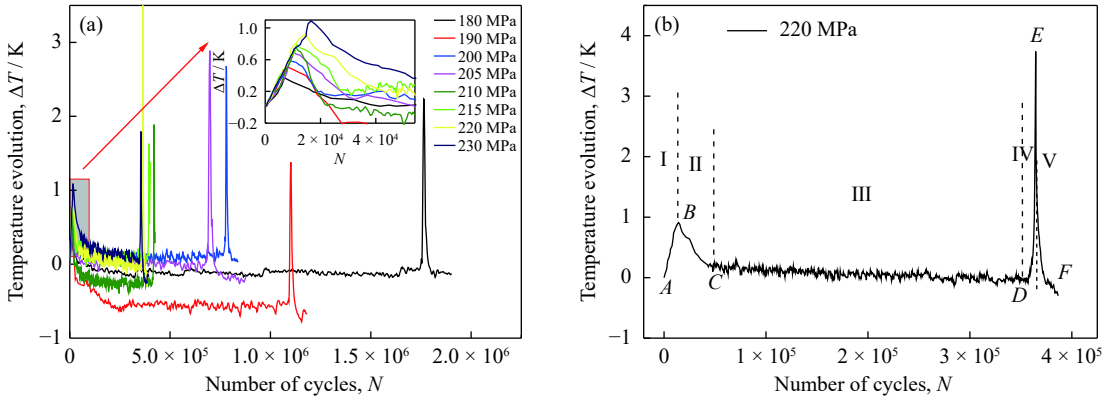

Fig. 6. Temperature evolution of the 6061 aluminum under maximum cyclic loadings of (a) ≥180 MPa and (b) 220 MPa. The insert figure in (a) is enlarged view of temperature change in the first stage.

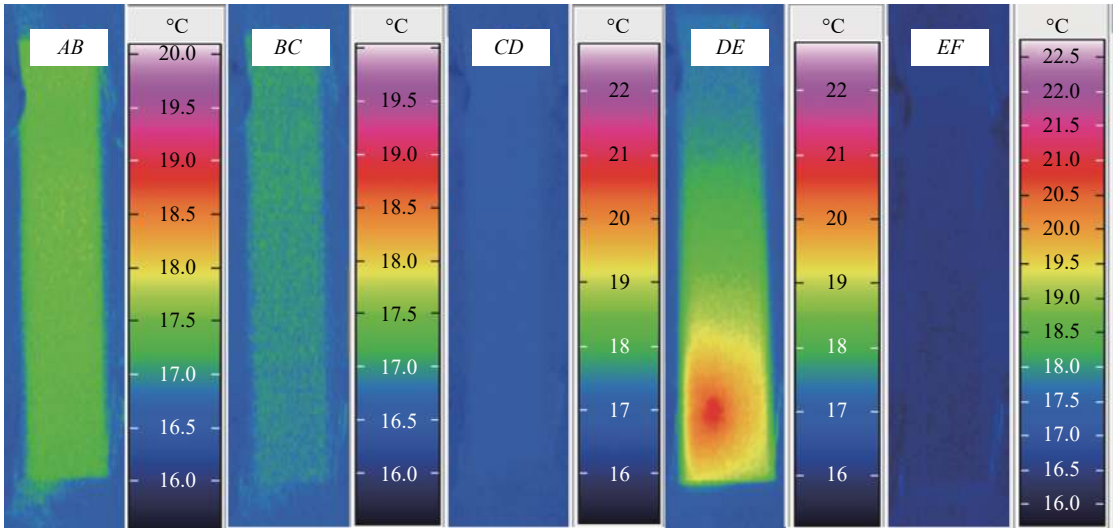

Fig. 7. The instantaneous infrared thermograms of the 6061 aluminum under maximum cyclic loading of 220 MPa, corresponding to the five temperature evolution stages shown in the Fig. 6(b).

3.4. Ratcheting strain of the 6061 aluminum alloy

The ratcheting strain as a function of the number of cycles under 220 MPa maximum loading is shown in Fig. 8(a). The ratcheting strain experiences three stages: I—initial rapid increase stage (<10000–12000 cycles), II —steady stage (12000–150000 cycles), and III—final abrupt increase stage (>150000 cycles). Fig. 8(b) shows the ratcheting strain of the 6061 aluminum alloy in stages I and II under different asymmetric maximum cyclic loadings from 70 to 220 MPa. The steady ratcheting strain difference ($\Delta\varepsilon_{(r,i)}$) increases with in-

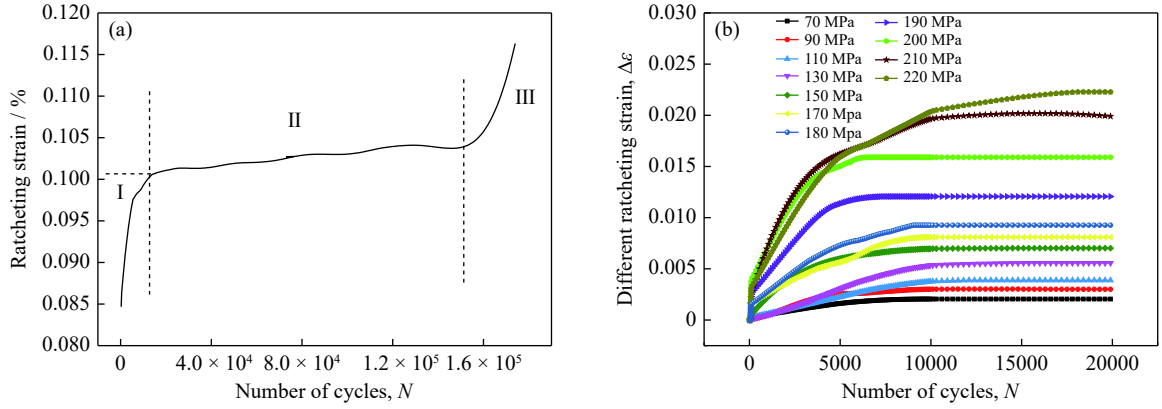

Fig. 8. Ratcheting strain curves of the 6061 aluminum under maximum cyclic loadings of (a) 220 MPa and (b) ≥70 MPa.

creasing cyclic loading. The $\varepsilon_{(r,i)}$ at cycle "i" which means the ratcheting strain, is defined as [24]:

$$\varepsilon_{(r,i)} = \frac{\varepsilon_{(i,max)} + \varepsilon_{(i,min)}}{2} \quad (7)$$

where $\varepsilon_{(i,max)}$ and $\varepsilon_{(i,min)}$ are the maximum and minimum of axial strain at cycle "i." The ratcheting strain difference $\Delta\varepsilon_{(r,i)}$ for comparison purpose is used and is defined as:

$$\Delta\varepsilon_{(r,i)} = \varepsilon_{(r,i)} - \varepsilon_{(r,1)} \quad (8)$$

where $\varepsilon_{(r,i)}$ and $\varepsilon_{(r,1)}$ are the ratcheting strain of the cycle "i" and cycle "1".

The ratcheting effect during cyclic loading caused the accumulation of damage and the failure. Hysteresis loops at different cycles of the 6061 aluminum alloy under different maximum cyclic loadings can be divided to three types. Figs. 9(a)–9(c) show the three types of hysteresis loop under maximum cyclic loadings of 50, 130, and 210 MPa, which respectively represent the hysteresis loops under the maximum cyclic loading range of ≤70, 80–180, and ≥180 MPa. Fig. 9 indicates that when the maximum cyclic loading is below 70 MPa, the accumulation of damage does not occur, so the corresponding hysteresis loop is approximately a line and almost overlapping; when the maximum cyclic loading is between 80 and 180 MPa, the area of the hysteresis loop narrows in the initial five cycles, and with the increasing number of cycles, the hysteresis loops shift to the right slightly and partially overlap, indicating the accumulation of plastic damage; when maximum cyclic loading is higher than 180 MPa, the hysteresis loops shift right more obviously and are more stable, indicating more serious plastic deformation and damage accumulated as defined by the ratcheting effect.

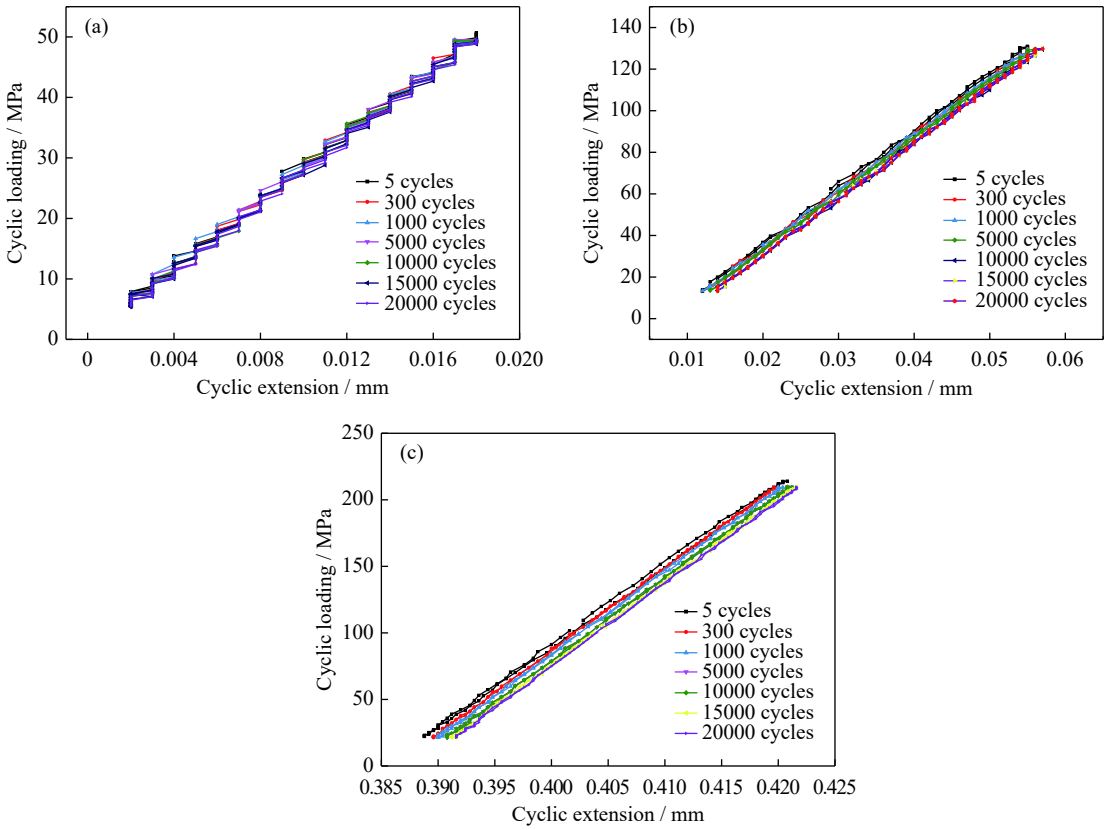

Fig. 9. Hysteresis loop at different cycles of the 6061 aluminum alloy under maximum cyclic loadings of (a) 50 MPa, (b) 130 MPa, and (c) 210 MPa.

3.5. Estimation of the fatigue limit based on infrared thermography and the steady ratcheting effect

The S–N curve (S is stress or cyclic loading, N is cyclic number) is shown in Fig. 10. According to the linear fitting, the fatigue limit is 170 MPa at 10^7 cycles.

Fig. 11 shows the two methods to estimate the fatigue limit based on IRT and the steady ratcheting effect. The linear fitting of the max temperature in stage I of Fig. 6(a) and the cyclic strength is shown in Fig. 11(a). The red line $L_{B'C}$ is linear fitting of the temperature corresponding to the cyclic loading below fatigue limit, and the blue line L_{CD} is the linear fitting of the temperature corresponding to the cyclic loading above the fatigue limit. The abscissa of the intersection of the two lines is 173 MPa, which is the fatigue limit predicted by IRT.

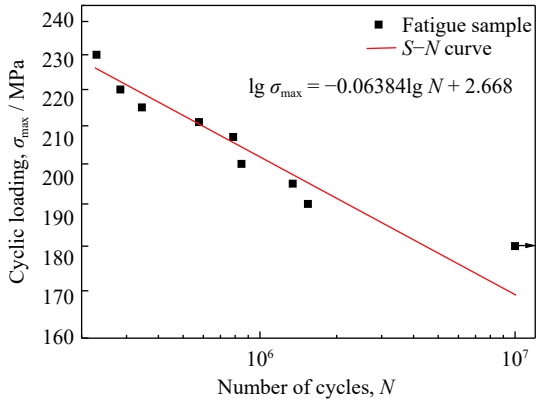

Fig. 10. Traditional *S–N* curve of the 6061 aluminum alloy.

The fatigue limit can be estimated at a cyclic loading level at which the ratcheting strain steady difference has a marked change, such as the case of the temperature evolution of the material. Fig. 11(b) shows the curves of the steady ratcheting strain difference $\Delta\varepsilon$ at 20000 cycles under different cyclic loadings. The steady ratcheting strain difference increases with the increase in cyclic loading, but at different rates. The L_{CD} shows a higher slope indicating clear damage under cyclic loading above the fatigue limit and L_{BC} shows a lower slope indicating light damage under cyclic loading below the fatigue limit. The abscissas of the intersection point, which is related to the different levels of damage, can be used to estimate the fatigue limit. Therefore, the cyclic loading corresponding to the intersection point *C* (177 MPa) can be estimated as the fatigue limit of the material.

According to Fig. 11, when the cyclic loading is in the range of elastic range, the temperature decreases and no ratcheting strain is observed (in stage I). When the cyclic loading is above the critical value (point *B*), the temperature increased and fatigue damage occurred, so point *B* can be called the cyclic elastic limit. There is an obvious increase in both temperature and steady ratcheting strain in L_{CD}. Therefore, the cyclic strength at the intersection point *C* is called the cyclic yield limit. Furthermore, the crack initiation and propagation are directly related to the plastic deformation [25]. The cyclic strength at point *C* corresponds to the fatigue limit at cycle of 10^7.

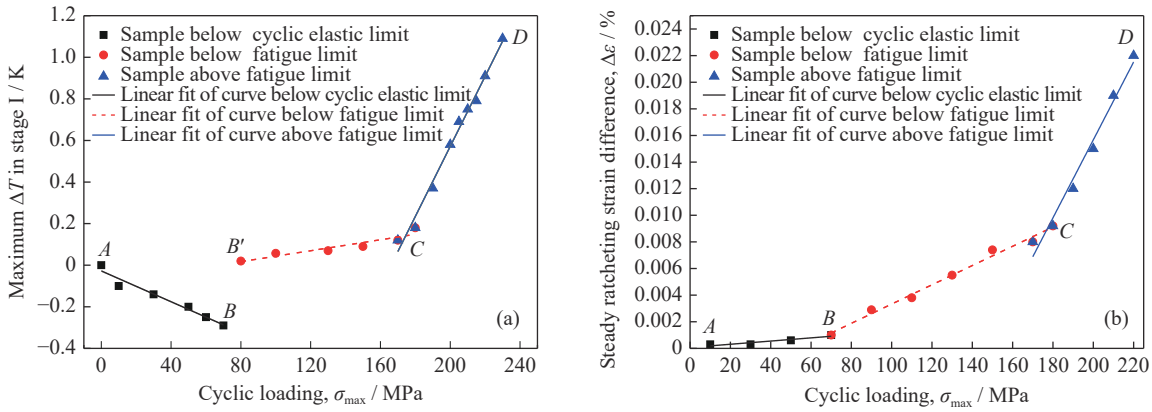

Fig. 11. Fatigue limit estimation based on (a) the maximum temperature increase in the first stage and (b) the ratcheting strain steady value.

4. Conclusions

In this study, the mechanism of the temperature evolution and ratcheting strain of the 6061 aluminum alloy under cyclic loading were investigated. Two methods were used to estimate the fatigue limit based on steady ratcheting strain difference and IRT. The conclusions can be summarized as follows.

(1) The temperature evolution of 6061 aluminum alloy under static tensile stress undergoes four stages: almost linear decrease, steep increase, abrupt increase, and finally a drop stage. Due to the thermoelastic effect, the temperature is nearly a linear decrease in the first stage.

(2) Under cyclic loading above 180 MPa, the temperature evolution of 6061 aluminum alloy undergoes five stages: initial increase, reversing decrease, stability, abrupt increase, and finally a drop stage; the ratcheting strain undergoes three stages: initial rapid increase, steady stage, and final increase stage. An obvious increase in temperature and ratcheting strain correspond to the final fatigue fracture.

(3) Based on the linear fitting of the temperature evolution and steady ratchet stability difference with cyclic loading, respectively, the three-line fitting was established. The fatigue limit estimated based on temperature evolution is 173 MPa, and based on the steady ratcheting strain difference is 177 MPa, which is in good agreement with 170 MPa from the traditional S–N curve. The two methods based on temperature increase and steady ratcheting strain difference can quickly

predict the fatigue limit to save time and cost.

Acknowledgements

This work was financially supported by the National Natural Science Foundation of China (Nos. 51505322 and 51775366) and the Natural Science Foundation of Shanxi Province, China (No. 201801D221137).

References

[1] Y.Q. Chen, S.P. Pan, M.Z. Zhou, D.Q. Yi, D.Z. Xu, and Y.F. Xu, Effects of inclusions, grain boundaries and grain orientations on the fatigue crack initiation and propagation behavior of 2524-T3 Al alloy, *Mater. Sci. Eng. A*, 580(2013), p. 150.

[2] J.C. Williams and E.A. Starke, Progress in structural materials for aerospace systems, *Acta. Mater.*, 51(2003), No. 19, p. 5775.

[3] T.M. Roberts and M. Talebzadeh, Fatigue life prediction based on crack propagation and acoustic emission count rates, *J. Constr. Steel Res.*, 59(2003), No. 6, p. 679.

[4] L. Zhang, X.S. Liu, S.H. Wu, Z.Q. Ma, and H.Y. Fang, Rapid determination of fatigue life based on temperature evolution, *Int. J. Fatigue*, 54(2013), p. 1.

[5] S. Bagavathiappan, B.B. Lahiri, T. Saravanan, J. Philip, and T. Jayakumar, Infrared thermography for condition monitoring—A review, *Infrared Phys. Technol.*, 60(2013), p. 35.

[6] J.L. Fan, X.L. Guo, and C.W. Wu, A new application of the infrared thermography for fatigue evaluation and damage assessment, *Int. J. Fatigue*, 44(2012), p. 1.

[7] Z.Q. Cui, H.W. Yang, W.X. Wang, Z.F. Yan, Z.Z. Ma, B.S. Xu, and H.Y. Xu, Research on fatigue crack growth behavior of AZ31B magnesium alloy electron beam welded joints based on temperature distribution around the crack tip, *Eng. Fract. Mech.*, 133(2015), p. 14.

[8] Z.Q. Xu, H.X. Zhang, Z.F. Yan, F. Liu, P.K. Liaw, and W.X. Wang, Three-point-bending fatigue behavior of AZ31B magnesium alloy based on infrared thermography technology, *Int. J. Fatigue*, 95(2017), p. 156.

[9] Z.F. Yan, H.X. Zhang, P.D. Chen, and W.X. Wang, Anisotropy of fatigue behavior and tensile behavior of 5A06 aluminum alloy based on infrared thermography, *J. Wuhan Univ. Technol.-Mater. Sci. Ed.*, 32(2017), No. 1, p. 155.

[10] C.F.C. Bandeira, P.P. Kenedi, L.F.G. Souza, and S. de Barros, On the use of thermographic technique to assess the fatigue performance of bonded joints, *Int. J. Adhes. Adhes.*, 83(2018), p. 137.

[11] W.P. Yang, X.L. Guo, Q. Guo, and J.L. Fan, Rapid evaluation for high-cycle fatigue reliability of metallic materials through quantitative thermography methodology, *Int. J. Fatigue*, 124(2019), p. 461.

[12] K. Dutta and K.K. Ray, Ratcheting phenomenon and post-ratcheting tensile behavior of an aluminum alloy, *Mater. Sci. Eng. A*, 540(2012), p. 30.

[13] R. Kreethi, P. Verma, and K. Dutta, Influence of heat treatment on ratcheting fatigue behavior and post ratcheting tensile properties of commercial aluminum, *Trans. Indian Inst. Met.*, 68(2015), No. 2, p. 229.

[14] S. Sreenivasan, S.K. Mishra, and K. Dutta, Ratcheting strain and its effect on low cycle fatigue behavior of Al 7075-T6 alloy, *Mater. Sci. Eng. A*, 698(2017), p. 46.

[15] S.K. Mishra, H. Roy, and K. Dutta, Influence of ratcheting strain on tensile properties of A356 alloy, *Mater. Today: Proc.*, 5(2018), No. 5, p. 12403.

[16] Y.C. Lin, Z.H. Liu, X.M. Chen, and Z.L. Long, Cyclic plasticity constitutive model for uniaxial ratcheting behavior of AZ31B magnesium alloy, *J. Mater. Eng. Perform.*, 24(2015), No. 5, p. 1820.

[17] Y.C. Lin, X.M. Chen, Z.H. Liu, and J. Chen, Investigation of uniaxial low-cycle fatigue failure behavior of hot-rolled AZ91 magnesium alloy, *Int. J. Fatigue*, 48(2013), p. 122.

[18] B. Yang, P.K. Liaw, M. Morrison, C.T. Liu, R.A. Buchanan, J.Y. Huang, R.C. Kuo, J.G. Huang, and D.E. Fielden, Tempreature evolution during fatigue damage, *Intermetallics*, 13(2005), No. 3-4, p. 419.

[19] B. Yang, P.K. Liaw, J.Y. Huang, R.C. Kuo, J.G. Huang, and D.E. Fielden, Stress analyses and geometry effects during cyclic loading using thermography, *J. Eng. Mater. Technol.*, 127(2005), No. 1, p. 75.

[20] H.T. Lee and G.H. Shaue, The thermomechanical behavior for aluminum alloy under uniaxial tensile loading, *Mater. Sci. Eng. A*, 268(1999), No. 1-2, p. 154.

[21] B. Yang, G. Wang, W.H. Peter, P.K. Liaw, R.A. Buchanan, D.E. Fielden, Y. Yokoyama, J.Y. Huang, R.C. Kuo, J.G. Huang, and D.L. Klarstrom, Thermal-imaging technologies for detecting damage during high-cycle fatigue, *Metal. Mater. Trans. A*, 35(2004), No. 1, p. 15.

[22] Y.T. Zhang, *Theory of Thermo-Viscoelasticity*, Tianjin University Press, Tianjin, 2002.

[23] K.S. Anish and P.V. Pillai, Stress pattern analysis using thermal camera, *Int. J. Adv. Prod. Mech. Eng.*, 2(2016), No. 5, p. 5.

[24] Y.C. Lin, Z.H. Liu, X.M. Chen, and J. Chen, Uniaxial ratcheting and fatigue failure behaviors of hot-rolled AZ31B magnesium alloy under asymmetrical cyclic stress controlled loadings, *Mater. Sci. Eng. A*, 573(2013), p. 234.

[25] Z.F. Yan, D.H. Wang, X.L. He, W.X. Wang, H.X. Zhang, P. Dong, C.H. Li, Y.L. Li, J. Zhou, Z. Liu, and L.Y. Sun, Deformation behaviors and cyclic strength assessment of AZ31B magnesium alloy based on steady ratcheting effect, *Mater. Sci. Eng. A*, 723(2018), p. 212.